JOURNAL OF PROPULSION AND POWER
Vol. 16, No. 3, May–June 2000

Wall Drag in Internal Mach-2 Flow with Cavity and Transpiration Injection

Linda A. Castiglone*
University of Washington, Seattle, Washington 98195
G. Burton Northam† and Ned R. Baker‡
NASA Langley Research Center, Hampton, Virginia 23681
and
Larry A. Roe§
University of Arkansas, Fayetteville, Arkansas 72701

A drag-measurement facility was used to evaluate potential scramjet fuel-injection/wall-cooling configurations. Mach-2 airflow containing a train of weak, unsteady, reflecting shocks was supplied to test plates equipped with force and static-pressure instrumentation. A nonporous flat plate, a partially porous flat plate, and a wall cavity plate (the latter two with mass injection) were tested. The nonporous plate results were within 10% of both theoretical and numerical predictions. The porous plate exhibited reduced drag (relative to the nonporous flat plate), even without mass addition, caused by pressure equalization across the impinging shocks. Addition of mass decreased the drag 46% relative to the flat-plate value. The rectangular wall cavity had a geometric aspect ratio (length in flow direction to depth) of 5.0. The cavity plate produced the highest drag of the cases tested. Without secondary injection cavity-plate drag exceeded the instrumentation range, but was estimated as higher than the flat plate by approximately one order of magnitude. A minimum amount of secondary flow injected into the cavity reduced the drag to a value 50% higher than the flat plate. Further cavity mass addition increased the drag. The porous flat plate provided drag reduction, whereas the cavity configuration demonstrated drag penalties when compared to the flat plate.

Introduction

SCRAMJETS are the propulsion system of choice for hypersonic transportation systems. As skin-friction and wave-drag losses are significant performance limiters in scramjet combustors, proper design requires efficient fuel injection, mixing, and flameholding, with minimum internal drag. This experimental program investigated the combined skin friction/wave drag of candidate combustor wall configurations and evaluated the impact of mass-addition techniques on the total drag. All tests were conducted in the Transverse Jet Facility located at NASA Langley Research Center in Hampton, Virginia. In these experiments, an air-bearing-load cell measurement system was employed to measure the combined skin friction and wave drag of flat, transpiration, and cavity plates in a shock-filled Mach 2 airstream. Both the transpiration and cavity plate could operate with or without mass addition. As baseline for the test program, a nonporous flat plate was the first and last configuration tested.

Nonporous flat-plate skin-friction drag has been thoroughly investigated[1–5] over the years. During the 1950s, van Driest,[6,7] among others, sought a theoretical solution to the skin-friction problem by solving the continuity, momentum, and energy differential equations, eventually leading to the van Driest II Theory[7] in 1956. His solution to the differential equations is still in general use today for viscous compressible boundary layers and calculation of skin-friction coefficients[8,9] and is used as a validation for this experimental program.

Transpiration (typically approximated by discrete hole injection) is a technique of mass addition that has been in use for decades as a way to cool surfaces exposed to high-temperature environments and is currently of interest for scramjet combustor cooling and friction reduction. In this experiment, a fabricated porous laminated plate, manufactured by Allison Engine Company and known as Lamilloy®, was used to distribute the flow across the model surface. No references were found in the open literature addressing the drag-reduction performance of Lamilloy. Transpiration surfaces are usually employed primarily as a thermal barrier in propulsion and reentry applications.[10–14] Drag reduction has generally been given secondary consideration because, until now, the value of transpiration as an effective thermal barrier outweighed any expected drag performance benefit or penalty within the intended applications.

A plate with a cavity was also evaluated. As illustrated in Fig. 1, a cavity flow structure is formed when a flow stream passes over a cavity or depression in a solid surface. The flow separates from the (upstream) rearward-facing step forming a shear layer. Flowfield structure, shock waves, reattachment points, and other specific flow details are strongly dependent on the size and shape of the cavity and the flow regime (open or closed cavity) of interest. In a closed cavity the flow separates from the rearward-facing step, impinges on the cavity floor or wall, and forms a complex characteristic shock and expansion structure, which is known to provide the highest total drag. In an open cavity flow the shear layer forms on the rearward-facing step, then crosses the span of the cavity, reattaching downstream of the forward-facing step. The reattachment of the flow forms a compression shock on the forward-facing step that propagates into the main flow stream. The shear layer generally bends toward the cavity floor, strengthening the expansion wave and shock structures and increasing the drag penalty.

A sketch of the optimum flowfield of a cavity flow, balanced with cavity mass addition (blowing), is shown in Fig. 1c. For blown-cavity operation the addition of mass alters the expansion fan and shock-wave system, offering the potential for significant drag reduction. Accomplished through the creation of a single vortex within the cavity, the cavity recirculation produces an effect that might be described as an aerodynamic roller-bearing. Reviews[15,16] of cavity investigations and research until 1990 are available, with other studies[17,18] conducted more recently.

During this investigation, a single plate representative of each candidate wall design concept was constructed, instrumented, and

Presented as Paper 97-2891 at the AIAA/ASME/SAE/ASEE, 33rd Joint Propulsion Conference, Seattle, WA, 6–9 July 1997; received 20 October 1997; revision received 2 April 1999; accepted for publication 26 May 1999.

*Doctoral Research Assistant. Senior Member AIAA.
†Research Scientist. Senior Member AIAA.
‡Principal Engineer.
§Assistant Professor. Senior Member AIAA.

tested. In an actual combustor the mass added to the cavity or introduced via transpiration would typically be fuel; air was used in this series of tests.

Experimental Apparatus and Methods

Facilities

The Langley Mach 2.0 Transverse Jet Facility is connected to a high-pressure, ambient-temperature air source, with a plenum chamber providing flow mixing and straightening. A converging-diverging nozzle accelerates the air to Mach 2 at the test section inlet. For this test program the air system supplied the wall-drag test tunnel with a constant airflow at 115 psia (793 kPa) nominal total pressure and an ambient total temperature of approximately 70°F (21°C). A separate 1000-psia (6895-kPa) air supply was used for transpiration and cavity injection.

Test Article and Design Parameters

Figure 2 presents a side-view drawing of the installed and assembled wall-drag test tunnel. The base unit consisted of an aluminum box within which were mounted an air-bearing suspension system and load cells for drag force measurement. The test plate, free floating in the axial direction, was mounted to the air-bearing system with brackets to form one side of the test section. The remainder of the test section was enclosed with aluminum and Plexiglas®. All aluminum surfaces were blackened to minimize any optical reflections, while the Plexiglas allowed optical access to the test-section flowfield for schlieren photography. The test section measured 1.52 in. (3.86 cm) high, 3.46 in. (8.79 cm) wide, and 8.5 in. (21.59 cm) long. Both the metric surface and the top plate were instrumented with wall static-pressure taps along the centerline and at two locations outboard of the centerline of the test article. The pressure in the plate gaps was also measured. The metric surface of the wall-drag test tunnel was composed of a fore plate, the test plate, and an end plate. The top plate was canted at a 0.65-deg divergence angle to provide a neutral pressure gradient within the test apparatus. Air bearings and load cells used to measure the axial forces are shown in Fig. 3.

Three test plates were designed and built: a nonporous flat plate, a transpiration plate, and a cavity plate that incorporated mass injection. Each plate was 3.45 in. (8.76 cm) wide, 4.50 in. (11.4 cm) long, mounted on the air-bearing system between stationary upstream and downstream plates, and instrumented with 12 static-pressure taps. The nonporous flat plate yielded baseline drag data, providing both a foundation for the remainder of the test program and a validation of the test system, as a well-known and extensively analyzed configuration.

The porous flat plate incorporated a transpiration region that spanned the width of the test section. The blown area began 0.755 in. (1.92 cm) downstream of the test plate leading edge and extended

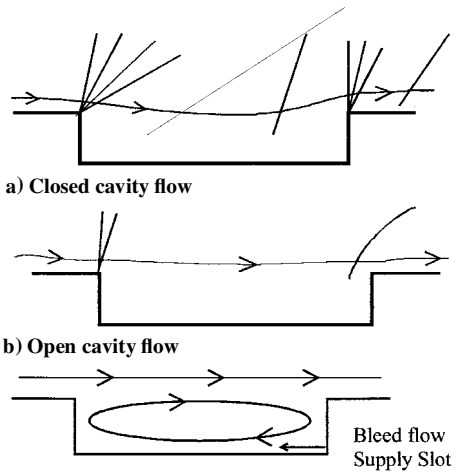

Fig. 1 Supersonic cavity flowfield modes: a) closed, b) open, and c) optimized.

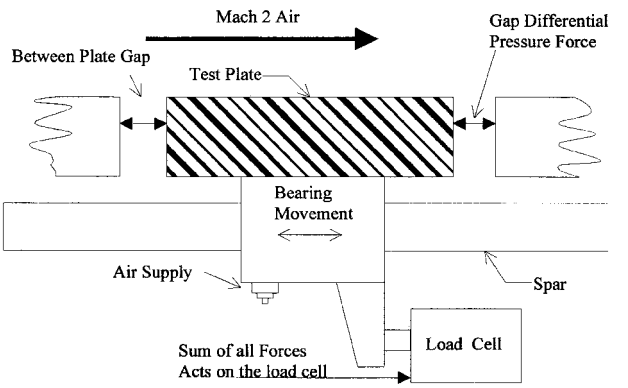

Fig. 3 Force balance composed of the test plate and suspension system.

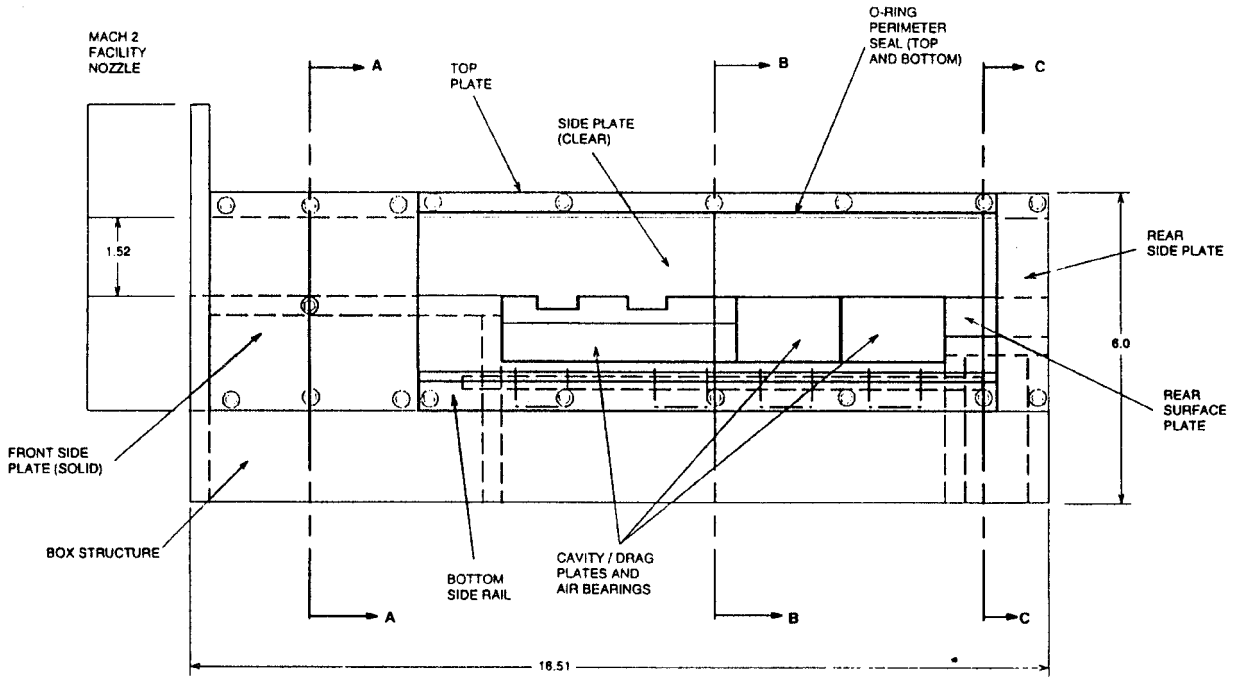

Fig. 2 Skin-friction drag Mach-2 test article.

1.25 in. (3.17 cm) in the flow direction. This region was covered with a Lamilloy plate that was epoxied over the injection manifold and fed by the facility air system. Lamilloy is a two-ply laminate of Haynes 188 plates with an evenly distributed surface hole pattern and a manifolding action that allows for an evenly distributed injection flow. A cutaway view of the two-ply Lamilloy sheet used in this experiment is presented in Fig. 4. Air enters a staggered series of holes on the bottom laminate from the pressurized manifold, then flows through a miniature distribution manifold and exits a set of offset staggered orifices in the top laminate, passing into the boundary layer of the main flow stream.

The cavity test plate (Fig. 5) had a rectangular cavity located in the same relative position as the transpiration plate. The 1.25 in. (3.18 cm) length in the flow direction and the 0.250 in. (0.64 cm) depth provide an aspect ratio (L/d) of 5.0, which generates an open-cavity flowfield in unblown operation. For blown operation (which, in an actual combustor, could be either air injection, fuel injection, or combined fuel-injection/flameholding), air can be injected into the cavity via a 0.020-in. (0.051-cm) high slot spanning the cavity at the bottom of the forward-facing step, as shown schematically in Fig. 1c. The cavity plate incorporated wall static-pressure taps along the centerline and pressure taps within the cavity.

Instrumentation

Drag measurements were made using load cells rated to ±10 lbf (44.5 N). The vertical design of the test article allowed the load cells to measure the weight of the plates and associated brackets and instrumentation prior to the initiation of main airflow. Total drag was determined by measuring the load cell forces and adding the static weight of the test article and the resultant force created by the between-plate gap pressures.

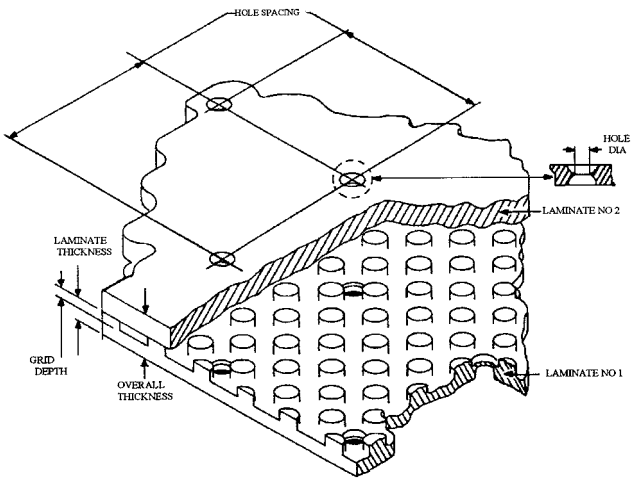

Fig. 4 Detailed drawing of the Lamilloy transpiration plate.

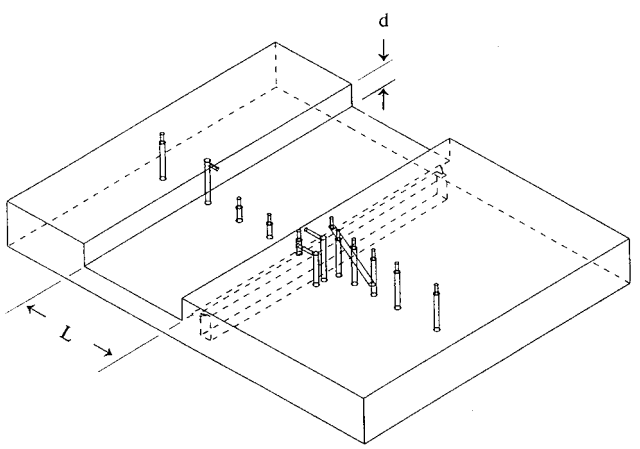

Fig. 5 Cavity-plate isometric view showing pressure tap locations.

Flowfield images were obtained by using the focusing schlieren imaging technology developed by Weinstein.[19] This allowed qualitative evaluation of the flowfield structure including general location of shocks or expansion fans and their relationships to the metric surface and mass-injection locations. Flow unsteadiness caused the shock waves to rapidly shift position, producing a smeared image. As a result, although the images produced were valuable for evaluating the general flowfield, only one has been incorporated into this document to provide a general visualization of the shock structure in the test section.

Results and Discussion

Drag Predictions

The van Driest II (Ref. 7) model was applied to predict drag loading for the flat-plate configuration using the method and equations described in White.[9] The properties for Mach-2 air were derived from the nominal total flow conditions: $P_T = 115.0$ psia (793 kPa) and $T_T = 529.7$ R (294 K). A one-dimensional isentropic analysis provided entrance-plane flow conditions. The results of this drag analysis at the nominal tunnel operating conditions yield a drag coefficient of $C_f = 1.81 \times 10^{-3}$ and a drag force of 1.65 lbf (7.34 N) for the flat plate.

An additional computational fluid dynamic (CFD) analysis of the facility nozzle, as well as the flat plate, was conducted using the CAN-DO[20] CFD code. The solution included a complete numerical solution of the flowfield from nozzle entrance plane to test-article exit plane. The analysis was for compressible, viscous, and turbulent flow, while ignoring real-gas effects. The calculated drag was 18.3% lower than that determined by the van Driest II model.

Flat Plate

The flat-plate configuration was tested at the beginning of the experiment as a baseline and again at the end of the experiment as an anchor. A statistical analysis of the 17 independent drag measurements showed the average total drag on the plate to be 1.47 ± 0.22 lbf (6.54 ± 0.97 N) within two standard deviations. This uncertainty of ±15% was estimated to be representative of the uncertainty for all acquired drag determinations for comparative analysis. The van Driest II analysis was 10.7% higher than the experimentally determined value, whereas the CAN-DO prediction was 7.5% lower. The conclusion was made that the flat-plate data matched both predictive methods, providing a validation of the experimental approach.

Wall-pressure distributions were collected during all tests to evaluate test conditions representative of structures in the main flow and to define the test-article pressure gradient. Figure 6 presents the metric surface wall-static-pressure distribution for a sample case. The measured pressure profile shows the effect of the reflecting shocks and is generally as predicted by the CFD model. The wall-static-pressure measurements are found to lie very close to the predicted curve for the first 3.5 in. (8.9 cm) of the duct. The differences after this axial position are caused by the 0.65-deg divergence angle of the actual test section, compared to the straight configuration evaluated in the earlier CFD analysis.

A focusing schlieren image of the test-section flowfield is shown in Fig. 7, with the flow from the bottom of the figure to the top. The overall test-section imaging area starts at a distance of 4.0 in. (10.2 cm) from the nozzle exit and continues for 11.5 in. (29.2 cm), whereas the test section height is 1.5 in. (3.8 cm). The flowfield is seen to contain weak shock waves reflecting back and forth across the test section duct at the Mach-line angle of approximately 30 deg. Mottling within the image is caused by background image imperfections that could not be compensated.

Transpiration Plate

To evaluate the effect of surface injection on total drag, the transpiration plate was tested at the same main flow conditions as the flat plate, both with and without injection. The unblown transpiration plate had an average total drag of 1.27 lbf (5.64 N), which is 13.6% less than that of the average total drag measured for the flat-plate.

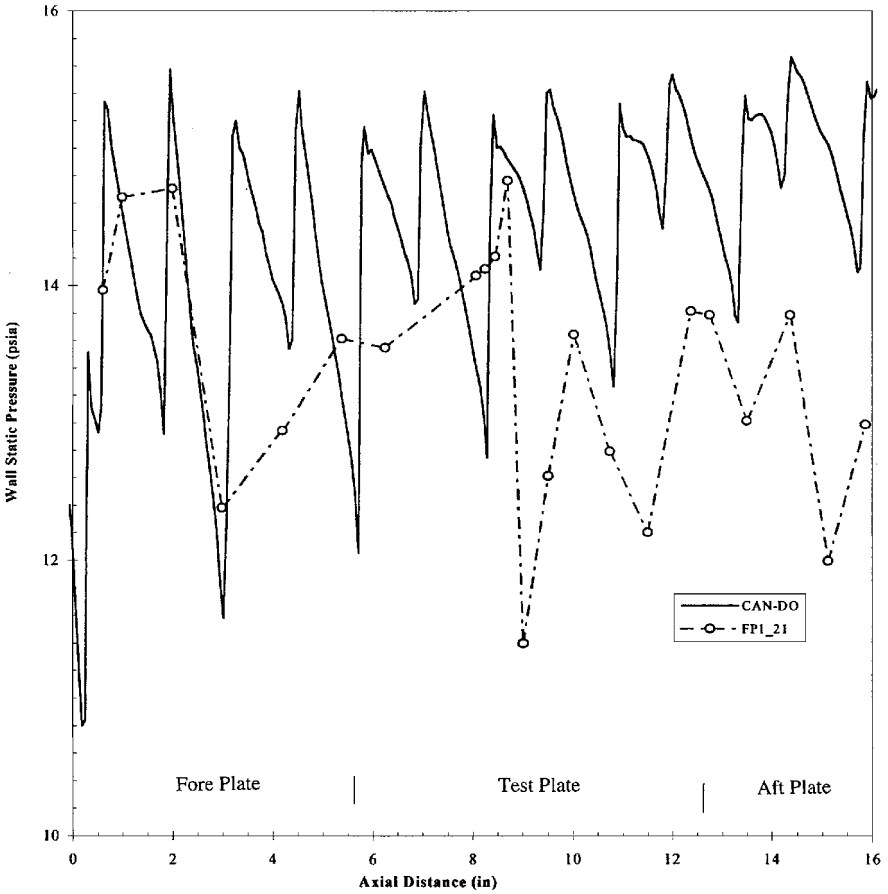

Fig. 6 Flat-plate static-pressure distributions—CFD results (CAN-DO) and experimental (FP1_21).

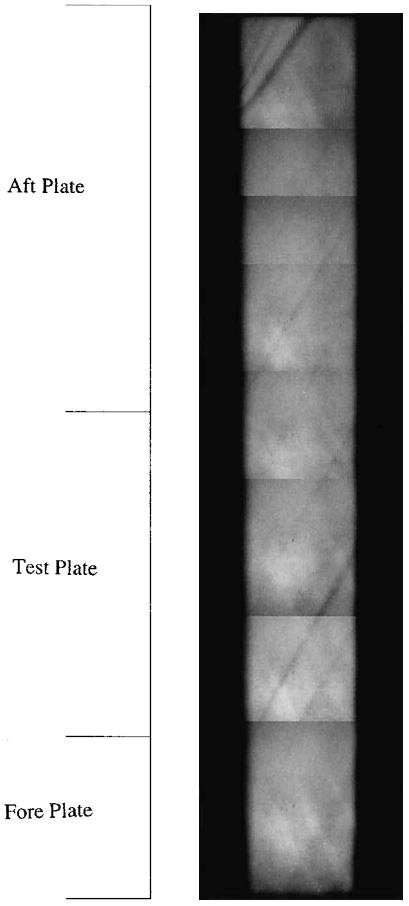

Fig. 7 Schlieren image of flowfield, nonporous flat plate.

This difference is 1.8 times the calculated standard deviation observed in the flat-plate data and is considered a valid trend in the data. The unblown transpiration plate is essentially a flat plate containing a vented cavity. The venting allows the pressures to equalize across the shock reflection, potentially reducing drag. The transpiration plate drag decreased steadily with increasing mass addition, eventually attaining a maximum 38% reduction in measured drag, relative to the flat plate, at the maximum flow rate tested.

In the transpiration plate experimental phase, wall-static-pressure data were collected on both the metric surface and the top plate of the test article (Fig. 8). Although the static-pressure data provide discontinuous distributions, the conclusion can be made that the mass addition significantly altered the flowfield structure in the test section. The highest-injection test suggests that a major flow alteration had taken place within the flowfield, which is supported by the fact that the measured pressure at the downstream end of the test plate shows a dramatic increase relative to the values at lower injection rates.

An evaluation of the schlieren images showed that three major shock structures were produced: one by the fore plate-test plate interface and one each at the upstream and downstream seams where the Lamilloy was epoxied into the test plate. The flowfield structure was observed to change little at the low mass-addition rates. At the higher flow rates the downstream seam wave angle was found to increase progressively with increasing injectant flow.

Cavity Plate

The cavity-plate tests evaluated the use of blown cavities to reduce drag in supersonic flow. This cavity-plate design was expected to provide an open cavity flowfield (Fig. 1) without mass addition because previous investigations have shown open cavity flow to transition to closed cavity flow above an L/d of 11.0, putting the unblown test article ($L/d = 5.0$) well within the open cavity range.

Drag data were obtained for all but the unblown case. The cavity-test phase was started with a zero-injection condition test, which

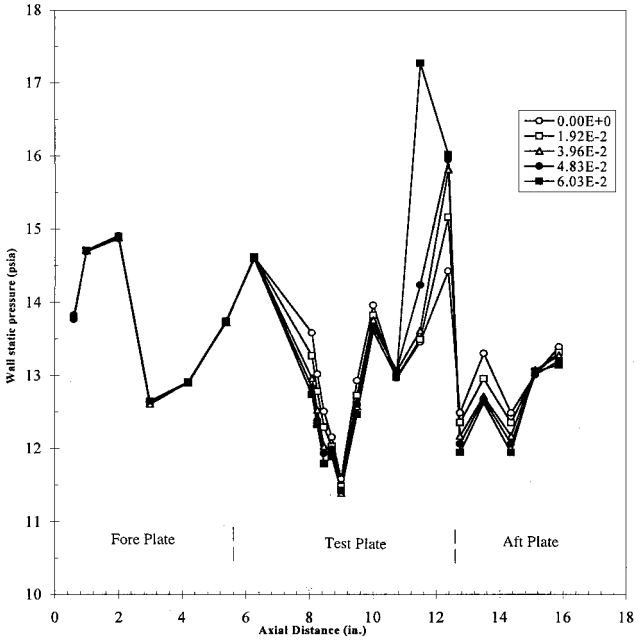

Fig. 8 Transpiration-plate wall-static-pressure distribution for five injection-to-main mass-flow ratios.

developed force levels that exceeded the limits of the load cells. Analysis of the acquired data showed that the sum of forces on the unblown cavity plate was no less than 23 lbf (102 N) during steady-state operation. The addition of the smallest meterable amount of secondary injection reduced the total drag by at least 90%. Beyond this point, however, the addition of more mass into the cavity increased the drag.

The static pressures for the cavity plate are included as Fig. 9. The wall-static-pressure distribution in the fore-plate region is shown to be unaffected by the mass addition for all injection flow rates tested. An apparent strengthening of the shock wave emanating from the rearward-facing step (with increasing mass addition) is seen to affect the pressures in the downstream portion of the test section. There the wall static pressure is seen to increase, especially in the maximum injection case.

Five wall static pressures were instrumented within the cavity itself: one on the rearward-facing step, three on the cavity floor, and two equally spaced and slightly offset from the centerline on the forward-facing step and above the air injection slot. These intra-cavity pressure measurements are plotted in Fig. 10 vs surface distance, rather than axial length, to conveniently represent measurements within the cavity itself. The increase in wall static pressure with increasing mass addition in the upstream half of the cavity was as expected, whereas the pressures in the downstream half of the cavity shifted with the addition of mass. The unblown case has the highest force in the drag direction because the downstream wall pressures are much higher than the upstream wall pressure. This pressure distribution was altered by the addition of mass, shifting the pressure forces within the cavity until the forces were nearly balanced at the highest injection condition. Although this trend does not explain all of the noted drag variation, it does contribute to understanding of the physical phenomena evidenced by these experimental results. The physical limitations of the experimental model prevented additional pressure instrumentation within the cavity that would have provided increased resolution. This pressure distribution was not similar to the standard open-cavity and closed-cavity pressure distributions, which tend to increase through the cavity, as described by Wilcox.[21]

Assessments of the schlieren images showed a shock reflecting within the cavity, which would create a higher pressure on the forward-facing step and increase the indicated drag, consistent with the very high measurements observed without air injection into the cavity. The introduction of injected air disrupted the reflecting shock structure, dislodging the shock wave that had been reflecting from the forward-facing step in the unblown case. The reflected shock angle upstream of the cavity remained constant for all cases; however, image comparison shows the angle of the shock emanating from the rearward-facing step decreased with increased mass addition. The shift in shock structure is also apparent in the wall-static-pressure distributions (Fig. 10).

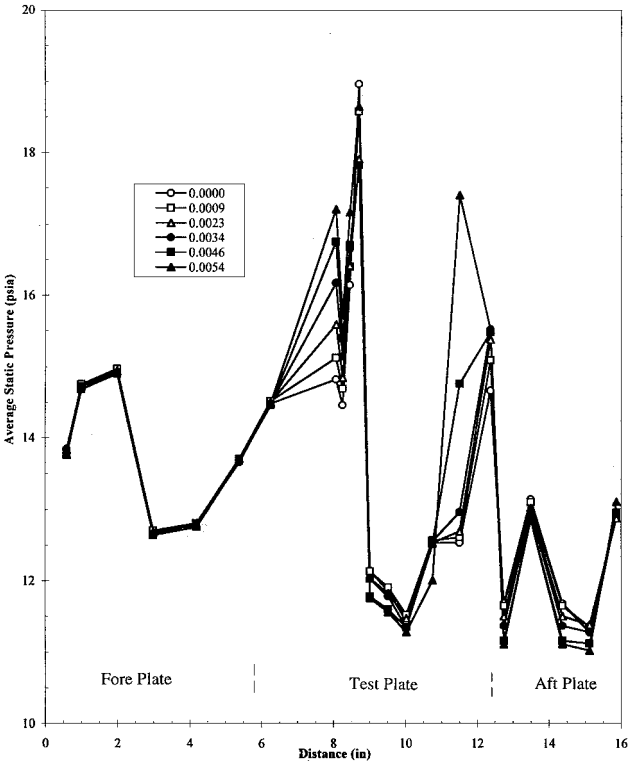

Fig. 9 Cavity-plate wall-static-pressure distributions for six injection-to-main mass-flow ratios.

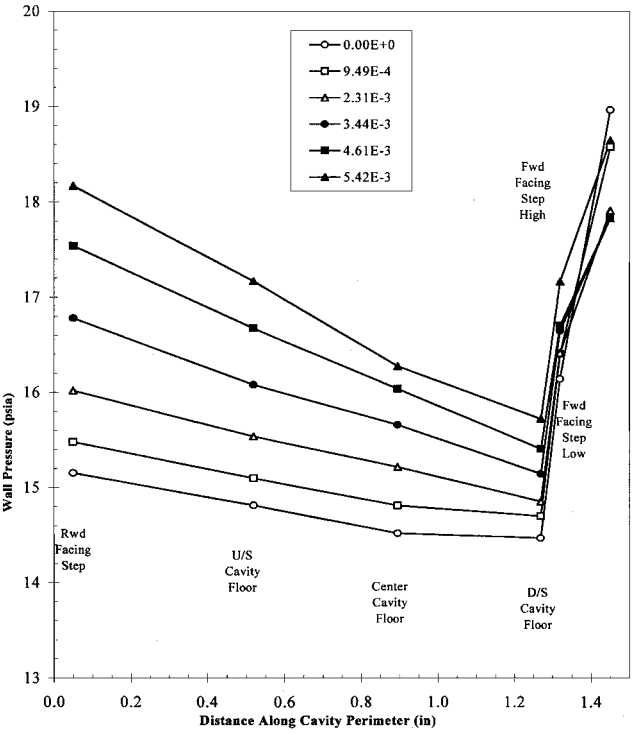

Fig. 10 Intra-cavity wall static pressures for the cavity plate at six injection-to-main mass-flow ratios.

Drag Comparison

The drag trends are clarified in Fig. 11, where total drag is plotted as a function of mass-flow-rate ratio (injected-to-main) for all of the

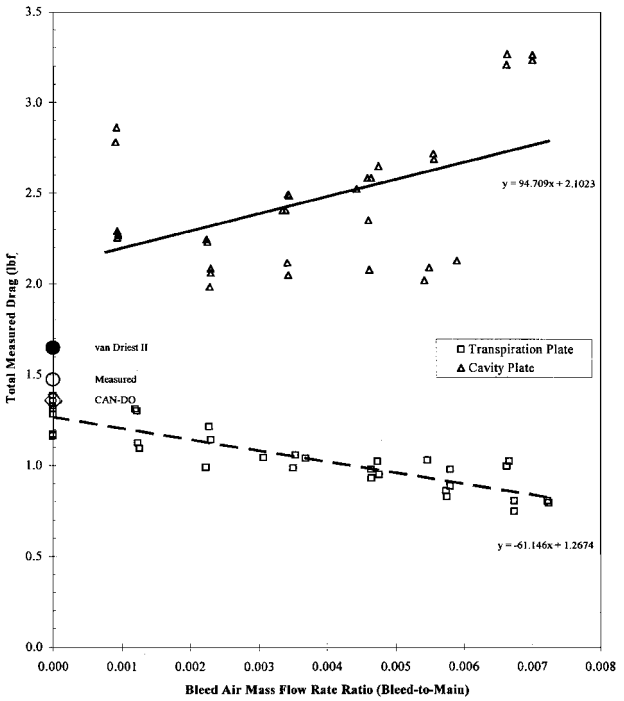

Fig. 11 Calculated drag for the flat-plate configuration and experimentally determined drag for all configurations tested.

plate tests. A linear curve fit was applied to both the transpiration plate and blown-cavity plate data (excluding the zero-injection condition). The transpiration plate is seen to exhibit lower drag than the nonporous flat plate under all test conditions studied, with drag decreasing linearly with increasing injection. The high scatter in the cavity-plate data is believed to be caused by small (and uncontrolled) test-to-test variations in shock location. The flat plate and transpiration plate are less sensitive to shocks and thus do not display this variation in drag results. This condition of variable shock location should also be expected to exist in actual flight combustors. Recognizing that the unblown cavity plate exhibited an estimated drag of 23 lbf (102 N), the data illustrate that the total drag decreased dramatically with even small amounts of secondary injection and then increased with increasing injection.

Conclusions

The primary goal of this experimental program was to determine if the addition of mass could alter the internal drag characteristics of a scramjet combustor operating at Mach 2. A drag-measurement system intended to measure the integrated effect of all the drag forces on a plate was designed, manufactured, installed, and made operational. This system was capable of secondary mass injection, direct force measurement, wall-static-pressure measurement, and flowfield imaging.

Three plate configurations were tested for drag characteristics: a flat plate, a porous flat plate, and a cavity plate. Flat-plate results indicated the average total drag to be within 10.7% of the van Driest II prediction and within 7.5% of the results of the CFD analysis. The lowest drag determined experimentally was for the transpiration plate operating at maximum injection. The measured drag of this configuration was 0.80 lbf (3.6 N), 46% lower than the flat-plate drag. The results indicate that drag decreased with increasing mass injection. Focusing schlieren and wall-static-pressure data helped to evaluate the flowfield structures responsible for the reduction in drag.

The cavity-plate drag performance provided unique results because of the characteristics of the shock flowfield. The unblown flow condition severely over-ranged the load cells, and total drag was estimated to be in excess of 23 lbf (102 N). Addition of the smallest measurable amount of mass flow reduced the measured total drag to 2.4 lbf (10.7 N). This dramatic reduction was caused by the disruption of a shock wave that was reflecting from the forward-facing step of the cavity. Additional injection beyond this point increased the drag. A cavity wall configuration intended for drag reduction should only be used in a controlled environment as a weak shock wave can cause severe loading. These forces must be anticipated in preliminary design considerations for supersonic combustors.

The shock structures can be considered a nonoptimum or off-design condition that may be encountered in flight applications of these wall configurations. We demonstrated that, although the flat plate was relatively unaffected by the introduction of shock structures, cavities can experience severe loading if exposed to even weak shock waves. Although it may be possible to design an optimized cavity that provides significant drag reduction, nonoptimal flow conditions could conceivably cause drag forces on the order of 10 times flat-plate levels.

Acknowledgment

This work was sponsored by the Hypersonic Propulsion Branch, NASA Langley Research Center, Hampton, Virginia.

References

[1]Schlicting, H., *Boundary Layer Theory*, McGraw–Hill, New York, 1968, pp. 597–606.

[2]Liepmann, H., and Dhawan, S., *Direct Measurement of Local Skin Friction in Low-Speed and High-Speed Flow*, First U.S. National Congress of Applied Mechanics, Chicago, 1951, pp. 869–874.

[3]Coles, D., "Direct Measurement of Supersonic Skin Friction," *Journal of the Aeronautical Sciences*, Vol. 19, No. 10, 1952, p. 717.

[4]Coles, D., "Measurements of Turbulent Friction on a Smooth Flat Plate in Supersonic Flow," *Journal of the Aeronautical Sciences*, Vol. 21, No. 7, 1954, pp. 433–448.

[5]O'Donnell, R. M., "Experimental Investigation at a Mach Number of 2.41 of Average Skin-Friction Coefficients and Velocity Profiles for Laminar and Turbulent Boundary Layers and an Assessment of Probe Effects," NACA TN 3122, Jan. 1954.

[6]van Driest, E. R., "Turbulent Boundary Layer in Compressible Fluids," *Journal of the Aeronautical Sciences*, Vol. 18, No. 3, 1951, pp. 145–160.

[7]van Driest, E. R., "On Turbulent Flow Near a Wall," *Journal of the Aeronautical Sciences*, Vol. 23, No. 11, 1956, pp. 1007–1036.

[8]Hopkins, E. J., and Inouye, M., "An Evaluation of Theories for Predicting Turbulent Skin Friction and Heat Transfer on Flat Plates at Supersonic and Hypersonic Mach Numbers," *AIAA Journal*, Vol. 9, No. 6, 1971, pp. 993–1003.

[9]White, F. M., *Viscous Fluid Flow*, 2nd ed., McGraw–Hill, New York, 1991, p. 550.

[10]Rubesin, M. W., "The Influence of Surface Injection on Heat Transfer and Skin-Friction Associated with the High Speed Boundary Layer," NACA TM RM A55L13, Feb. 1956.

[11]Romanenko, P. N., Kharchenko, V. N., and Semenov, Y. P., "Effect on Heat Exchange and Friction of Coolant Supply in Turbulent Boundary Layer," *Journal of Engineering Physics*, Vol. 9, No. 6, 1965, pp. 816–833.

[12]Martellucci, A., "Effect of Mass Transfer on Hypersonic Turbulent Boundary Layer Properties," *AIAA Journal*, Vol. 10, No. 2, 1972, pp. 181–187.

[13]Andrews, G. E., Gupta, M. L., and Mcpadi, M. C., "Full Coverage Discrete Hole Film Cooling: Cooling Effectiveness," *International Journal of Turbo and Jet Engines 2*, 1985, pp. 199–212.

[14]Holden, M. S., Van Osdol, J., and Rodriguez, K. M., "An Experimental Study of Transpiration Cooling on the Distribution of Heat Transfer and Skin Friction to a Sharp, Slender Cone at Mach 11 and 13," AIAA Paper 90-0308, Jan. 1990.

[15]Emerson, D. A., and Poll, D. T. A., "Computation of Laminar Flow over Cavities," Ph.D. Dissertation, Div. of Aerospace Engineering, Univ. of Manchester, England, 1990.

[16]Komerath, N. M., Ahuja, K. K., and Chambers, F. W., "Prediction and Measurement of Flows over Cavities—A Survey," AIAA Paper 87-0166, Jan. 1987.

[17]Vakili, A. D., and Gauthier, C., "Control of Cavity Flow by Upstream Mass Injection," AIAA Paper 91-1645, June 1991.

[18]Soltani, S., and Hillier, R., "An Experimental and Computational Study of Hypersonic Cavity Flows," AIAA Paper 94-0766, Jan. 1994.

[19]Weinstein, L. M., "Large-Field High-Brightness Focusing Schlieren System," *AIAA Journal*, Vol. 31, No. 7, 1993, pp. 1250–1255.

[20]Korte, J. J., Kumar, A., Singh, D. J., and White, J. A., "CAN-DO, CFD-Based Aerodynamic Nozzle Design & Optimization Program for Supersonic/ Hypersonic Wind Tunnels," AIAA Paper 92-4009, July 1992.

[21]Wilcox, F. J., Jr., "Experimental Investigation of Porous-Floor Effects on Cavity Flow Fields at Supersonic Speeds," NASA TP 3032, Nov. 1990.